Magneto-structural correlations of a three-dimensional Mn based metal–organic framework†‡

Muhammad Arif Nadeem,[a] Donald J. Craig,[b] Roland Bircher[c] and John A. Stride*[a,c]

Received 30th October 2009, Accepted 3rd March 2010
First published as an Advance Article on the web 29th March 2010
DOI: 10.1039/b922750d

A 3D metal–organic framework, $[Na\{Mn_3(Hbtc)_2(btc)\}\cdot 5H_2O]_n$ (**1**) (H_3btc = 1,3,5-benzene tricarboxylic acid), was synthesized under hydrothermal conditions. The structure of **1** was established by single crystal X-ray diffraction analysis; **1** crystallizes in the monoclinic space group $P2/c$, a = 9.753(3) Å, b = 12.751(2) Å, c = 14.174(4) Å, β = 109.41(1)°. The complex **1** is isostructural to previously reported MIL-45 and consists of one dimensional wave like chains of carboxylate bridged hexa-coordinated Mn(II) ions. Variable temperature magnetic susceptibility measurements revealed dominant antiferromagnetic exchange interactions and the intra-chain exchange constants J_1 = -2.4 cm^{-1} and J_2 = -0.6 cm^{-1} compare well with literature values for similar materials. Inter-chain interactions are expected to be very small in this compound and there is no indication of magnetic ordering phenomena in the temperature range from 300–2 K.

Introduction

Metal–organic frameworks (MOFs) are crystalline hybrid inorganic–organic solids with structures composed of metal clusters with multidimensional nets or frameworks by organic linkers.[1] The crystal engineering of coordination frameworks has attracted great interest from chemists, not only due to the unusual topologies and interesting properties such as high surface area and porosity, but also to their potential applications in gas adsorption, ion-exchange, and catalysis technologies.[2,3] In particular, carboxylate containing ligands have drawn much attention in recent years owing to the diversity of the binding modes of carboxylate groups to metal atoms (Chart 1).

The studies reported to date suggest that the formation of coordination frameworks is influenced by many factors, including the nature of the ligands, the coordination geometry of the metal ions, the ratio between the metal salt and ligand, and the reaction conditions.[4]

In our effort to prepare new multifunctional MOFs we have focused on the ligand H_3btc. The three carboxylate groups of this ligand can adopt multiple coordination modes, which can affect the topology and magnetic properties of final product.[5,6] 1,3,5-benzene tricarboxylic acid (H_3btc) has been used successfully by other groups to prepare a broad variety of MOFs with intriguing magnetic and gas adsorption properties.[7] In this paper we describe the synthesis, structural and magnetic properties of the new 3D compound $[Na\{Mn_3(Hbtc)_2(btc)\}\cdot 5H_2O]_n$ (**1**). The previously reported MIL-45, $K[M_3(BTC)_3]\cdot 5H_2O$ (M = Co and Fe) is isostructural to **1** which showed the ferromagnetic open framework[8] while we aim to study the antiferromagnetic framework of complex **1**.

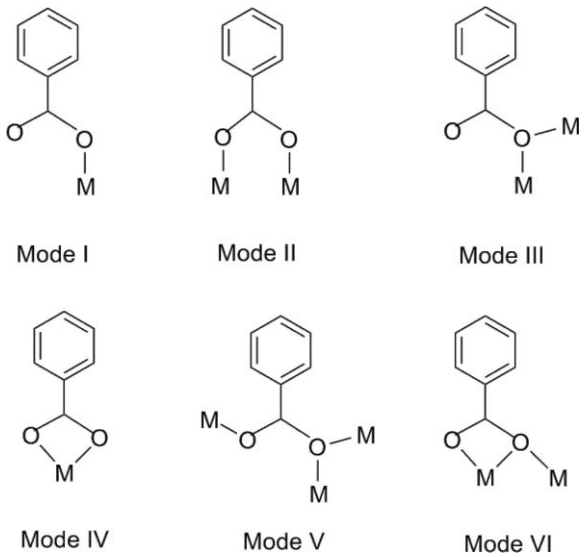

Chart 1 Binding modes of carboxylate ligands.

Experimental

Synthesis

A mixture of H_3btc (0.84 g, 4 mmol) and NaOH (0.48 g, 12 mmol) in 10 ml distilled water was stirred for 1 h, followed by addition of a solution of $MnCl_2\cdot H_20$ (0.25 g, 1.26 mmol) in 5 ml H_2O. The resulting solution was stirred for about 1 h at room temperature, then sealed in a 23 ml, teflon-lined, stainless steel autoclave and heated at 220 °C for three days under autogenous pressure. The

[a]*School of Chemistry, University of New South Wales, Sydney, NSW 2052, Australia. E-mail: j.stride@unsw.edu.au; Fax: +61 (02) 9385 6141; Tel: +61 (0)2 9385 4675*
[b]*Analytical Centre, University of New South Wales, Sydney, NSW 2052, Australia*
[c]*Bragg Institute, Australian Nuclear Science and Technology Organisation, PMB 1, Menai, NSW 2234, Australia*

† Dedicated to Dr Donald Craig.

‡ Electronic supplementary information (ESI) available: Fig. S1. CCDC reference number 752721. For ESI and crystallographic data in CIF or other electronic format see DOI: 10.1039/b922750d

Table 1 Crystallographic data for **1**

Empirical formula	$C_{27}H_{21}Mn_3NaO_{23}$
Formula weight	901.3
Temperature/K	294
Wavelength/Å	0.71073
Crystal system	Monoclinic
Space group	*P*2/*c*
a/Å	9.753(3)
b/Å	12.751(2)
c/Å	14.174(4)
β/°	109.41(1)
Volume/Å^3	1662.5(7)
Z	2
ρ/g cm^{-3}	1.80
Completeness to ≤ 25°	100.00%
Limiting indices	$0 \le h \le 11$ $0 \le k \le 15$ $-16 \le l \le 16$
Reflections number	3097
R_{int}	0.013
F_{000}	906.0
S	1.91
$R[F^2 > 2\sigma(F^2)]$	0.038
$wR(F^2)$	0.059

reaction mixture was then cooled to room temperature over a period of 4 h. Pink crystals of **1** suitable for single crystal X-ray diffraction analysis were collected from the final reaction mixture by filtration and dried in air at ambient temperature (52.8% yield based on manganese), Anal. calcd. $C_{27}H_{21}Mn_3NaO_{23}$: C 35.98%, Mn 18.28%. Found, C 37.15%, Mn 19.36%. FT-IR (KBr, cm^{-1}): 3409 brs, 2997 w, 1720 s, 1622 s, 1559 s, 1447 s, 1378 s, 1266 m, 1193 s, 1103 s, 1023 w, 938 w, 755 s, 715 s, 525 s, 461 s. The broad band at 3409 cm^{-1} is characteristic of the υ_{OH} of a protonated carboxylic group of Hbtc.[9] The TGA data of **1** showed an initial weight loss between 85 and 200 °C corresponding to the loss of coordinated water molecules, (exp% = 10, calc% = 9.9). The second weight loss at 350 °C is attributed to the loss of all btc ligands to yield Mn_3O_4 as residue.

Crystallographic analysis

A crystal of **1** was mounted on a glass fibre, and data was collected at 294 K on a Bruker kappa APEXII CCD area detector instrument. The diffractometer employs graphite monochromated Mo-Kα (0.7107 Å) radiation. The structure was solved by direct methods and all non-hydrogen atoms were refined by the full-matrix least-squares method. Hydrogen atoms on water molecules are shown in calculated positions. Details of crystal parameters, data collection and refinement are summarized in Table 1. The crystallographic data have been deposited in the CCDC and can be obtained free of charge from The Cambridge Crystallographic Data Centre *via* www.ccdc.cam.ac.uk/data_ request/cif quoting: CCDC-752721.‡

Magnetic measurements

Variable temperature magnetic susceptibility and magnetization measurements were performed with a Quantum Design PPMS EverCool system equipped with a vibrating sample magnetometer and a 9 T magnet. Data was collected on powdered crystals. The magnetic susceptibility measurements were performed for field-cooled and zero-field-cooled samples in magnetic fields of 0.1 T. Pascal's constants were used to estimate the diamagnetic corrections of **1**.[10] Magnetization data were collected in fields of up to 9 T, at three temperatures in the range between 2.0 and 10.0 K. A hysteresis loop measurement was performed at 2.0 K with saturation fields of ±7.0 T.

Results and discussion

Description of the structure

Compound **1** crystallizes in the monoclinic space group *P*2/*c*. Analysis of the single crystal X-ray diffraction data indicates two crystallographically distinct Mn(II) ions. The oxidation state was confirmed by bond valence sum calculations.[11] Both Mn(II) ions have an octahedral coordination environment, Fig. 1.

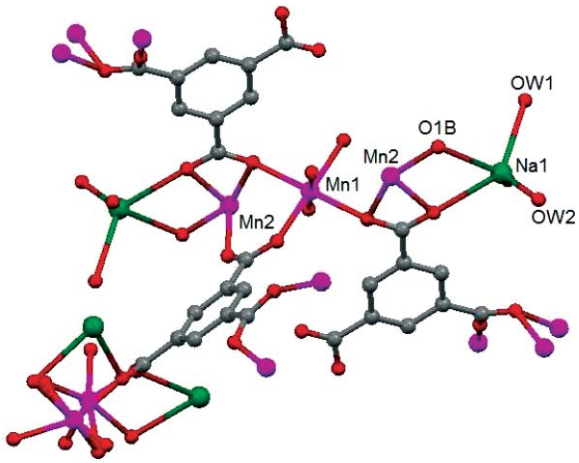

Fig. 1 Basic structural unit of compound **1** (hydrogen atoms are not shown for clarity).

Mn1 is located on an inversion centre and is coordinated with three pairs of oxygen atoms (Mn–O between 2.078(3) Å and 2.213(2) Å) belonging to four different Hbtc ligands and two different btc ligands. Mn2 is coordinated by 6 oxygen atoms (Mn–O between 2.105(3) Å and 2.410(3) Å) belonging to two different btc ligands and three Hbtc ligands. One of the latter acts in a bidentate chelating mode, whereas a second Hbtc ligand provides an additional loose bond with a Mn–O distance of 2.612(3) Å (Fig. 1 & 2). Selected bond distances and angles are listed in Table 2.

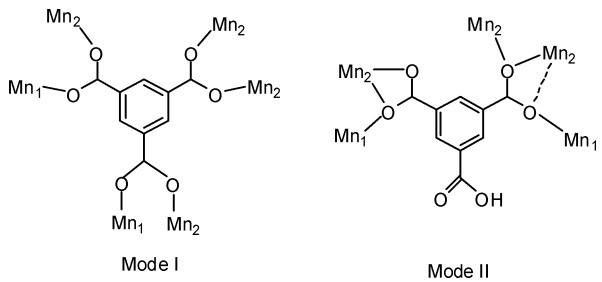

Fig. 2 Coordination modes of btc (left) and Hbtc (right) in complex.

Two Mn2 and a Mn1 ions are connected to form linear Mn_3 subunits with Mn1-Mn2 distances of 3.48 Å. Each Mn1-Mn2 pair is bridged by two *syn-syn* $\eta^1:\eta^1:\mu_2$ carboxylate groups of Hbtc and

Table 2 Selected bond lengths (Å) and bond angles (°) for compound **1**

Mn(1)-O(1A)	2.213(2)
Mn(1)-O(1A)	2.156(3)
Mn(1)-O(4A)	2.156(3)
Mn(1)-O(4A)	2.078(3)
Mn(1)-O(4B)	2.213(2)
Mn(2)-O(1A)	2.219(2)
Mn(2)-O(3A)	2.263(3)
Mn(2)-O(3A)	2.272(3)
Mn(2)-O(1B)	2.105(3)
Mn(2)-O(3B)	2.121(3)
O(1A)-Mn(2)	2.219(2)
O(3A)-Mn(2)	2.263(3)
O(3A)-Mn(2)	2.272(3)
O(4A)-Mn(1)	2.156(3)
O(3B)-Mn(2)	2.121(3)
O(1A)-Mn(1)-O(1A)	180.0(2)
O(1A)-Mn(1)-O(4A)	78.7(1)
O(1A)-Mn(1)-O(4A)	101.3(1)
O(1A)-Mn(1)-O(4B)	88.3(1)
O(1A)-Mn(1)-O(4B)	91.7(1)
O(1A)-Mn(1)-O(4A)	78.7(1)
O(1A)-Mn(1)-O(4B)	91.7(1)
O(1A)-Mn(1)-O(4B)	88.3(1)
O(4A)-Mn(1)-O(4A)	180.0(2)
O(4A)-Mn(1)-O(4B)	91.5(1)
O(4A)-Mn(1)-O(4B)	88.5(1)
O(4A)-Mn(1)-O(4B)	88.5(1)
O(4A)-Mn(1)-O(4B)	91.5(1)
O(4B)-Mn(1)-O(4B)	180.0(3)
O(1A)-Mn(2)-O(3A)	90.61(9)
O(1A)-Mn(2)-O(3A)	116.4(1)
O(1A)-Mn(2)-O(1B)	152.3(1)
O(1A)-Mn(2)-O(3B)	95.1(1)
O(3A)-Mn(2)-O(3A)	78.8(1)
O(3A)-Mn(2)-O(1B)	85.9(1)
O(3A)-Mn(2)-O(3B)	170.0(1)
O(3A)-Mn(2)-O(1B)	89.8(1)
O(3A)-Mn(2)-O(3B)	105.8(1)
O(1B)-Mn(2)-O(3B)	85.2(1)
Mn(1)-O(1A)-Mn(2)	103.7(1)
Mn(2)-O(3A)-Mn(2)	97.4(1)

btc ligands and a bridging-chelating $\eta^1{:}\eta^2{:}\mu_2$ carboxylate group of a second Hbtc ligand. This bridging geometry is very common in linear trinuclear Mn_3 clusters and Mn chains.[9,12] One of the bridging Hbtc carboxylate groups is coordinated to a Na ion, whereas the second carboxylate group of the Hbtc ligand joins two Mn_3 subunits *via* a monoatomic carboxylate bridge between neighbouring Mn2 ions. Additional links are provided by a second monoatomic carboxylate bridge from a Hbtc ligand and a *syn-syn* $\eta^1{:}\eta^1{:}\mu_2$ carboxylate bridge from btc. The linked Mn_3 subunits form wave like chains that lie along the crystallographic *c*-axis. Despite the large number of Mn carboxylate compounds in the literature, there are only very few reports of a bridging geometry with two monoatomic and only one *syn-syn* carboxylate, as present between the Mn_3 units in **1**.

The benzene rings of the btc ligands are stacked along the *a*-axis; two carboxylate groups provide bridges between Mn1 and Mn2 in the same chain, whereas the third carboxylate group bridges two Mn2 ions of neighbouring chains, linking them into 2D sheets parallel to the *bc*-plane (Fig. 3). The benzene rings of the Hbtc ligands are stacked in the *c*-direction. The two deprotonated carboxylate groups form a link between two neighbouring chains along *a*, thereby linking the 2D sheets into a three-dimensional structure. The closest Mn–Mn distances within and between

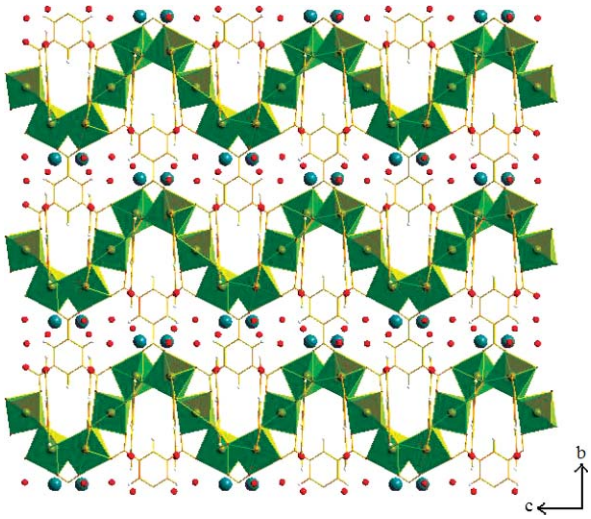

Fig. 3 View along *a* axis, the adjacent chains are separated by btc ligands to form two dimensional sheet on *bc* plane.

different 2D sheets are 8.08 Å and 8.15 Å, respectively. Moreover, each chain is surrounded by eight neighbouring chains running parallel to the *c*-axis.

Magnetic properties

Variable temperature magnetic susceptibility data of **1** collected at 0.1 T is plotted in Fig. 4. $\chi_m T$ decreases gradually from 11.92 cm^3 K mol^{-1} at 300 K to 1.05 cm^3 K mol^{-1} at 2.0 K; the room temperature value is slightly lower than the spin-only value of 13.13 cm^3 K mol^{-1} for three non-interacting Mn(II) centres with $g = 2.0$. This behaviour is consistent with dominant antiferromagnetic (AFM) interactions. The temperature dependent susceptibility obeys the Curie–Weiss law in the temperature range 25–300 K with parameters θ = -20.1 K and C = 4.27 cm^3 K mol^{-1} per Mn(II).[9] This is further support for the predominantly AFM nature of the exchange interactions.

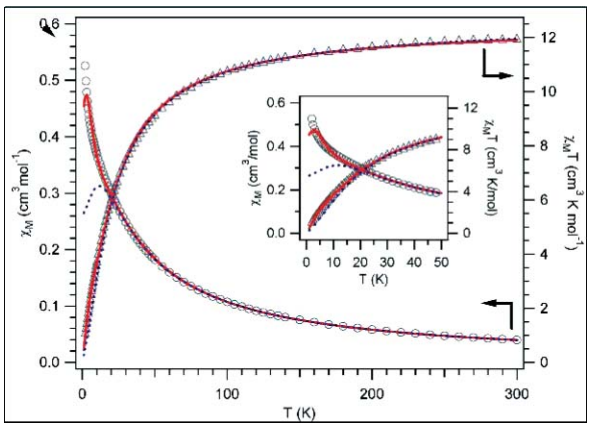

Fig. 4 Temperature dependent magnetic susceptibility of **1** shown as χ_m *vs.* T (circles) $\chi_m T$ *vs.* T (triangles). The insert shows a close-up of the low-temperature region. Dotted and solid lines correspond to the best fits obtained using eqn (2) and 4, respectively, with the parameters given in the text.

Table 3 Fit parameters for the linear chain models

Equation	g	J (Mn1-Mn2)/cm^{-1}	J (Mn2-Mn2)/cm^{-1}
(2)	1.96	-1.9	-1.9
(3)	1.97	-1.7	-1.7
(4)	1.95	-2.4	-0.6

The crystal structure of **1** suggests that the intra-chain interactions dominate the magnetic behaviour at elevated temperatures with inter-chain interactions expected to be much weaker due to the nature of the magnetic exchange path. In order to quantify the intra-chain exchange interactions, we have analysed the temperature dependent susceptibility data with various 1D chain models for isotropic Heisenberg chains. The determined parameters for all models correspond to an exchange Hamiltonian of the form

$$\mathbf{H}_{ex} = \sum -J_{ij}\,\mathbf{S}_i\mathbf{S}_j \qquad (1)$$

The magnetic susceptibility of an infinite chain of classical spins can be described by the analytical expression[9]

$$\chi_m = \frac{Ng^2\mu_B^2 S(S+1)}{3kT} \times \frac{(1+u)}{(1-u)} \qquad (2)$$

where $u = \coth[J\,S(S+1)/kT] - [kT/(J\,S(S+1))]$.

An alternative description of magnetic susceptibility is given by a parametric expression based on numerical results of Weng *et al.*[13] and coefficients determined by Hiller *et al.*:[14]

$$\chi_m = \frac{Ng^2\mu_B^2}{kT} \times \frac{(A+Bx^2)}{(1+Cx+Dx^3)} \qquad (3)$$

where $x = |J|/(2kT)$, $A = 2.9167$, $B = 208.04$, $C = 15.543$ and $D = 2707.2$.

The magnetic susceptibility data of **1** was fit using both models. Similar sets of parameters J and g were obtained (Table 3), with the first model giving a slightly better agreement to the data. However, both models were found to underestimate the data in the temperature range below 25 K. This deviation can be attributed to the fact that the experimental data does not show the maximum in χ_m typical for AFM chains as described by the two models. A further effort with a third model was therefore undertaken to better reproduce the experimental data. The Mn(II) chains in **1** comprise of two crystallographically distinct exchange interactions, forming an infinite exchange pattern $[J_1J_1J_2]_\infty$. J_1 and J_2 define the strength of the exchange interactions Mn1-Mn2 and Mn2-Mn2, respectively. A schematic of the exchange interactions upon the crystal structure for each of the models is shown in Figure S1 (Supporting Information‡). The magnetic susceptibility can be described as[15]

$$\chi_m = \frac{Ng^2\mu_B^2}{3kT} \times \frac{3(1-u_1^4u_2^2) + 4u_1(1-u_1^2u_2^2) + 2u_2(1-u_1)^2(1+u_1)^2 + 2u_1^2(1-u_2^2)}{(1-u_1^2u_2)^2} \qquad (4)$$

where $u_i = \coth[J_i\,S_i(S_i+1)/kT] - [kT/(J_i\,S_i(S_i+1))]$

The shape of the χ_mT *vs.* T curve of **1** clearly indicates that the dominant interactions are AFM in nature. The absence of a distinct minimum in the measured temperature range, further suggests that the second exchange constant is either only weakly ferromagnetic or is also antiferromagnetic in nature. A least-squares fit of the experimental data to eqn (4) indeed results in the parameter set $g = 1.95$, $J_1 = -2.4$ cm^{-1} and $J_2 = -0.6$ cm^{-1}. This model provides a good fit of χ_mT *vs.* T, that is significantly better below 25 K than that obtained with the previous models. Nevertheless there are still deviations at the lowest temperatures. The signs and strengths of the exchange interactions obtained with this model all lie in the same order of magnitude as values previously reported for carboxylate bridged Mn(II) chains and trimers.[7b,16,17,18] Only a few examples are available in literature on the exchange interactions between Mn(II) ions with two 1,1-μ_2 and one *syn-syn* 1,3-μ_2 carboxylate bridges.[19]

The determined parameters lead to a resulting spin of $S = 5/2$ per AFM coupled Mn_3 unit, which in turn is AFM coupled to the neighbouring Mn_3 units, to yield a spin ground state of $S = 0$. This is in good agreement with the slow and almost linear increase of the magnetization with increasing applied magnetic field (Fig. 4). At 2 K no magnetic hysteresis can be observed and no difference can be found between the zero-field cooled (ZFC) and field cooled (FC) susceptibility curves measured at 0.1 T. The absence of signs of magnetic order suggests that the inter-chain interactions are much smaller than the intra-chain interactions. The onset of inter-chain interactions is possibly responsible for the deviations observed between the models and the experimental data at the lowest temperatures.

Conclusion

A 3D coordination polymer $[Na\{Mn_3(Hbtc)_2(btc)\}\cdot 5H_2O]_n$ (**1**) has been synthesized under hydrothermal conditions. Infinite zig-zag $[Mn2\text{-}Mn1\text{-}Mn2]_n$ chains are linked by btc to form 2D layers, whereby each Hbtc bridges the 2D sheets to a three-dimensional structure. Compound **1** exhibits dominant antiferromagnetic interactions within the chain, while inter-chain interactions are expected to be very small, supported by the absence of such in the magnetization data. Finally compound **1** is stable up to 350 °C in air.

Notes and references

1 (*a*) S. L. James, *Chem. Soc. Rev.*, 2003, **32**, 276; (*b*) J. L. C. Rowsell and O. M. Yaghi, *Microporous Mesoporous Mater.*, 2004, **73**, 3; (*c*) N. W. Ockwig, O. Delgado-Friedrichs, M. O'Keeffe and O. M. Yaghi, *Acc. Chem. Res.*, 2005, **38**, 176.

2 (*a*) P. J. Hagrman, D. Hagrman and J. Zubieta, *Angew. Chem., Int. Ed.*, 1999, **38**, 2638; (*b*) R. Kitaura, K. Fujimoto, S.-I. Noro, M. Kondo and S. Kitagawa, *Angew. Chem., Int. Ed.*, 2002, **41**, 133; (*c*) S.-I. Noro, R. Kitaura, M. Kondo, S. Kitagawa, T. Ishii, H. Matsuzaka and M. Yamashita, *J. Am. Chem. Soc.*, 2002, **124**, 2568.

3 (*a*) S. R. Batten and R. Robson, *Angew. Chem., Int. Ed.*, 1998, **37**, 1460; (*b*) F. A. A. Paz and J. Klinowski, *Chem. Commun.*, 2003, 1484; (*c*) Y. Zhang, J. Li, J. Chen, Q. Su, W. Deng, M. Nishiura, T. Imamoto, X. Wu and Q. Wang, *Inorg. Chem.*, 2000, **39**, 2330.

4 (*a*) J. Fan, H.-F. Zhu, T.-a. Okamura, W.-Y. Sun, W- X Tang and N. Ueyama, *Chem.–Eur. J.*, 2003, **9**, 4724; (*b*) J. Fan, W.-Y. Sun, T-a. Okamura, W.-X. Tang and N. Ueyama, *Inorg. Chem.*, 2003, **42**, 3168; (*c*) W. Y. Sun, J. Fan, T. a. Okamura, J. Xie, K.-B. Yu and N. Ueyama, *Chem.–Eur. J.*, 2001, **7**, 2557.

5 (*a*) W. Zhang, S. Bruda, C. P. Landee, J. L. Parent and M. M. Turnbull, *Inorg. Chim. Acta*, 2003, **342**, 193; (*b*) M.-H. Zeng, M.-C. Wu, H. Liang, Y.-L. Zhou, X.-M. Chen and S.-W. Ng, *Inorg. Chem.*, 2007, **46**, 7241.

6 (*a*) E. Colacio, J. M. Domınguez-Vera, M. Ghazi, R. Kivekas, M. Klinga and J. M. Moreno, *Eur. J. Inorg. Chem.*, 1999, 441; (*b*) P. King, R. Clerac, C. E. Anson, C. Coulon and A. K. Powell, *Inorg. Chem.*, 2003, **42**, 3492; (*c*) D. Schulz, T. Weyhermüller, K. Wieghardt, C. Butzlaff and A. X. Trautwein, *Inorg. Chim. Acta*, 1996, **246**, 387.
7 (*a*) O. M. Yaghi, G. Li and H. Li, *Nature*, 1995, **378**, 703; (*b*) S. O. H. Gutschke, M. Molinier, A. K. Powell, R. E. P. Winpenny and P. T. Wood, *Chem. Commun.*, 1996, 823.
8 M. R-Cavellec, C. Albinet, C. Livage, N. Guillou, M. Nogues, J. M. Greneche and G. Ferey, *Solid State Sci.*, 2002, **4**, 267.
9 R. M. Silverstein and F. X. Webster, *Spectrometric Identification of Organic Compounds*, 6th edition, John Wiley & Sons, 1998.
10 O. Kahn, *Molecular Magnetism*. VCH Publishers Inc., New York, 1993.
11 N. E. Brese and M. O'Keeffe, *Acta. Cryst.*, 1991, **B47**, 192–197.
12 S. G. Baca, I. L. Malaestean, T. D. Keene, H. Adams, M. D. Ward, J. Hauser, A. Neels and S. Decurtins, *Inorg. Chem.*, 2008, **47**, 11108.
13 C. H. Weng, *Ph.D. Dissertation*, Carnegie-Mellon University, Pittsburgh, PA, 1968.
14 W. Hiller, J. Straehle, A. Datz, M. Hanack, W. E. Hatfield, L. W. Ter Haar and P. Guetlich, *J. Am. Chem. Soc.*, 1984, **106**, 329.
15 M. A. M. Abu-Youssef, M. Drillon, A. Escuer, M. A. S. Goher, F. A. Mautner and R. Vicente, *Inorg. Chem.*, 2000, **39**, 5022.
16 D. P. Kessissoglou, *Coord. Chem. Rev.*, 1999, **185–186**, 837.
17 M. J. Plater, M. R. St J. Foreman, R. A. Howie, J. M. S. Shakle, E. Coronado, C. J. Gomez-Garcia, T. Gelbrich and M. B. Hursthouse, *Inorg. Chim. Acta*, 2001, **319**, 159.
18 M. Xue, G. Zhu, Q. Fang, X. Guo and S. Qiu, *J. Mol. Struct.*, 2006, **796**, 165.
19 Z. J. Zhong and X.-Z. You, *Polyhedron*, 1994, **13**, 2157.

